JBMR Plus, 2024, **8**, ziae108
https://doi.org/10.1093/jbmrpl/ziae108
Advance access publication: August 4, 2024
Research Article

Girk3 deletion increases osteoblast maturation and bone mass accrual in adult male mice

Samantha R. Weaver[1], Haydee M. Torres[1], Katherine M. Arnold[1], Elizabeth L. Zars[1], Eduardo Peralta-Herrera[1], Earnest L. Taylor[2], Kanglun Yu[3], Ezequiel Marron Fernandez de Velasco[4], Kevin Wickman[4], Meghan E. McGee-Lawrence[3], Elizabeth W. Bradley[5], Jennifer J. Westendorf[1,6,*]

[1]Department of Orthopedic Surgery, Mayo Clinic, Rochester, MN 55905, United States
[2]Altis Biosystems, Durham, NC 27709, United States
[3]Department of Cellular Biology and Anatomy, Medical College of Georgia at Augusta University, Augusta, GA 30912, United States
[4]Department of Pharmacology, University of Minnesota, Minneapolis, MN 55455, United States
[5]Department of Orthopedics, School of Medicine, University of Minnesota, Minneapolis, MN 55455, United States
[6]Department of Biochemistry and Molecular Biology, Mayo Clinic, Rochester, MN 55905, United States

*Corresponding author: Jennifer J. Westendorf, Mayo Clinic, Department of Orthopedic Surgery, 200 First Street SW, Rochester, MN 55095, United States (westendorf.jennifer@mayo.edu)

Abstract

Osteoporosis and other metabolic bone diseases are prevalent in the aging population. While bone has the capacity to regenerate throughout life, bone formation rates decline with age and contribute to reduced bone density and strength. Identifying mechanisms and pathways that increase bone accrual in adults could prevent fractures and accelerate healing. G protein-gated inwardly rectifying K^+ (GIRK) channels are key effectors of G protein-coupled receptor signaling. *Girk3* was recently shown to regulate endochondral ossification. Here, we demonstrate that deletion of *Girk3* increases bone mass after 18 weeks of age. Male 24-week-old *Girk3*$^{-/-}$ mice have greater trabecular bone mineral density and bone volume fraction than wildtype (WT) mice. Osteoblast activity is moderately increased in 24-week-old *Girk3*$^{-/-}$ mice compared to WT mice. In vitro, *Girk3*$^{-/-}$ bone marrow stromal cells (BMSCs) are more proliferative than WT BMSCs. Calvarial osteoblasts and BMSCs from *Girk3*$^{-/-}$ mice are also more osteogenic than WT cells, with altered expression of genes that regulate the wingless-related integration site (Wnt) family. Wnt inhibition via Dickkopf-1 (Dkk1) or β-catenin inhibition via XAV939 prevents enhanced mineralization, but not proliferation, in *Girk3*$^{-/-}$ BMSCs and slows these processes in WT cells. Finally, selective ablation of *Girk3* from cells expressing Cre recombinase from the 2.3 kb-Col1a1 promoter, including osteoblasts and osteocytes, is sufficient to increase bone mass and bone strength in male mice at 24 weeks of age. Taken together, these data demonstrate that *Girk3* regulates progenitor cell proliferation, osteoblast differentiation, and bone mass accrual in adult male mice.

Keywords: osteoblasts, Wnt/β-catenin/lrps, osteoporosis, genetic animal models, microCT

Lay Summary

Osteoporosis is a prevalent, debilitating disease characterized by low bone mass. Identifying pathways that enhance bone formation could lead to therapies that prevent fractures and increase bone mass. In this study, we show that whole-body or osteoblast-specific deletion of G protein-gated inwardly rectifying K^+ channel 3 (*Girk3*) increases bone mass in male adult mice. Osteoblast progenitor cells from *Girk3*$^{-/-}$ animals are more proliferative and differentiate more quickly into mature osteoblasts. Taken together, we show that Girk3 is a novel regulator of bone mass in adult mice.

Received: June 28, 2024. **Accepted:** July 25, 2024

Graphical Abstract

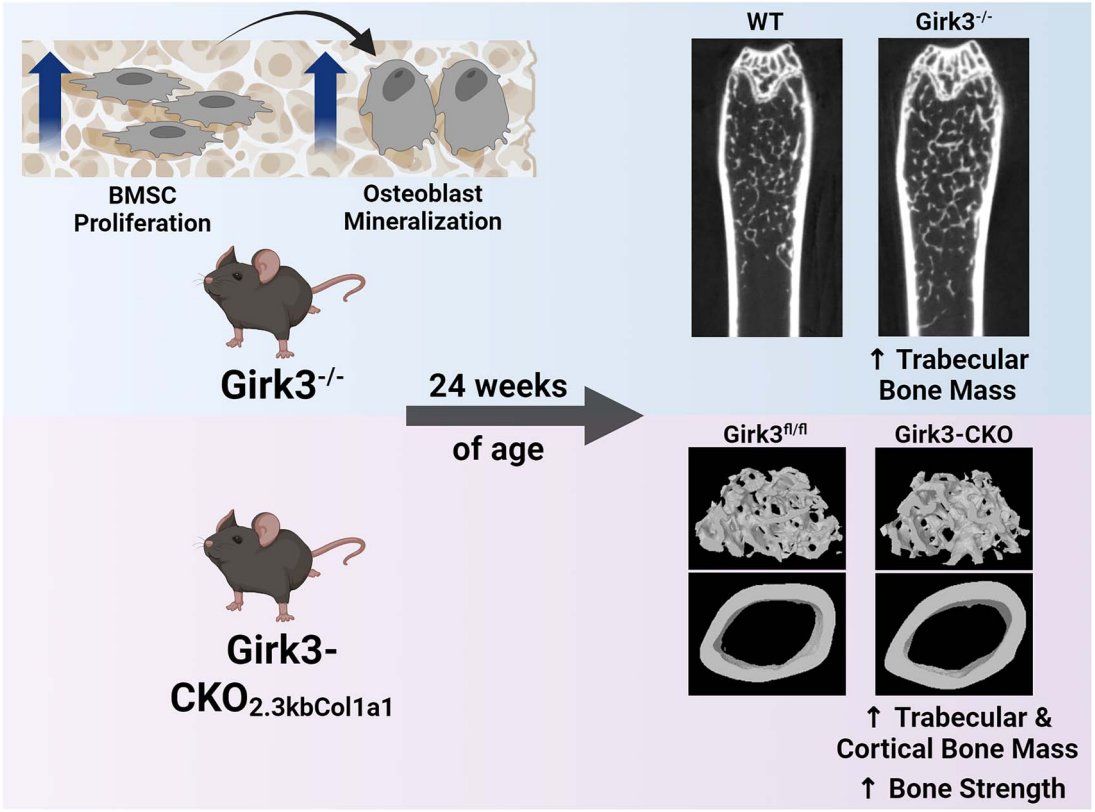

Introduction

Bone tissue is remodeled throughout life to maintain skeletal strength and physiological health. During adolescence and early adulthood, bone formation outpaces bone resorption. Peak bone mass is achieved by the second or third decade of life, with women reaching peak bone mass earlier than men.[1] It is estimated that up to 60% of the risk of osteoporosis, characterized by low bone mineral density (BMD), skeletal fragility, and increased risk of fracture, can be accounted for by the amount of bone acquired during development and into early adulthood.[2] Throughout the lifespan, stem cell populations become smaller and sex hormone levels decline, inducing periods of imbalance between bone formation and bone resorption.[3] The bone tissue may have difficulty recovering from excessive resorption, which leads to net bone loss for the rest of the lifespan and ultimately osteoporosis if left untreated.[4] As osteoporosis is generally considered a condition of aging, it is essential to identify processes that drive bone accrual in the mature, adult skeleton. This is particularly true for men, as male osteoporosis is understudied despite 1 in 5 men over the age of 50 suffering an osteoporotic fracture.[5] Few instances of adult-onset bone mass accrual in genetically modified mice have been reported.[6-8] In this study, we investigated the potential role of G protein-gated inwardly rectifying K^+ (GIRK) channel 3 as a key regulator of adult bone mass accrual.

GIRK channels allow for the flow of potassium ions across cell membranes in response to G protein coupled receptor (GPCR) activation. Mammalian GIRK channels are homo- and hetero-tetramers comprised of 4 subunits (GIRK1/*Kcnj3*, GIRK2/*Kcnj6*, GIRK3/*Kcnj9*, and GIRK4/*Kcnj5*). When GPCR ligands stimulate pertussis toxin-sensitive $G_{i/o}$–G proteins, the liberated $G\beta\gamma$ subunit binds to intracellular domains of GIRK channels, increasing their gating.[9,10] The subsequent efflux of K^+ reduces neuron and cardiomyocyte excitability.[11,12] In rodent models, modulation of GIRK channels affects addictive behavior, including dependence on alcohol[13] and opioids,[11] as well as pain.[14] GIRKs may also be therapeutic targets for human diseases, including epilepsy[15] and cardiac arrhythmia.[16] There are few studies characterizing the functions of GIRK channels in non-excitable cells. *Girk4* is associated with late-onset obesity[17] and primary aldosteronism.[18] *Girk2* deletion in a specific subset of hypothalamic neurons is associated with obesity after approximately 16 weeks of age.[19] Modulating GIRK channels also affects breast cancer cell survival and activity,[20] pancreatic islet cell physiology,[21] and platelet function.[22] In the musculoskeletal system, we reported that *Girk3* negatively regulates endochondral ossification, as *Girk3*$^{-/-}$ mice have longer femora and tibiae, potentially due to delayed vasculogenesis allowing for an extended period of growth.[23] Chondrocytes from *Girk3*$^{-/-}$ mice are also more responsive to kappa opioid signaling.[23]

The highly conserved Wnt family plays roles in embryogenesis, osteogenesis, as well as fat, lung, and kidney development.[24] Wnt proteins constitute a large family of secreted glycoproteins that activate canonical and non-canonical signaling in mesenchymal progenitor cells and other osteoblast lineage cells to regulate differentiation.[25] Wnt signaling can be inhibited by extracellular antagonists, including Dickkopf-1 (DKK1) and sclerostin (SOST), as well as by antagonists of intracellular signaling factors, such as the β-catenin inhibitor

XAV939.[24] SOST-neutralizing antibodies are FDA-approved for the treatment of osteoporosis.[26]

Our previous work showed that *Girk3* suppresses long bone growth in mice up to 12-weeks-old.[23] We observed no changes in bone mass between 4-week-old WT and *Girk3*$^{-/-}$ littermates. Here, we report that bone mass increases later in life in adult *Girk3*$^{-/-}$ mice. *Girk3*$^{-/-}$ mice diverge from wildtype (WT) littermates between 18- and 24-weeks-old. Bone marrow stromal cells isolated from adult *Girk3*$^{-/-}$ mice are more proliferative, have increased cell metabolic activity, and show greater mineralization in vitro, which can be partially prevented by inhibition of Wnt signaling via β-catenin inhibitors and Dkk1. Conditional deletion of *Girk3* in osteoblasts also increases bone mass only in adult mice, demonstrating that the effects of *Girk3* deletion are bone cell autonomous. Taken together, these data identify *Girk3* as a suppressor of adult bone mass accrual.

Materials and methods

Mice

All animals used for the current study were male mice. Female mice were also collected and are part of a separate analysis because they exhibit unique systemic phenotypes. *Girk3*$^{-/-}$ mice were described previously.[15,27] *Girk3*$^{fl/fl}$ mice were generated by crossing mice acquired from the Medical Research Council Harwell (strain: Kcnj9$^{tm1a(EUCOMM)Hmgu}$) with the C57BL/6 N flippase (Flp) deleter mouse (C57BL/6-Tg(ACTFLPe)) to remove the NEO cassette. The resulting mice were crossed with 2.3 kb-Col1a1-Cre mice,[28] which targets mature osteoblasts and osteocytes[28,29] to create conditional knockout (CKO) animals, *Girk3*-CKO$_{2.3Col1a1}$. Cre transgene presence was confirmed by PCR as previously described.[30] *Girk3* gene rearrangements were genotyped using the following primers: forward: 5'-TAATGTATATGATTACA CTGCC-3' and reverse: 5'-CAGACGTACATGAGGGCAAA-3'. The Mayo Clinic Institutional Animal Care and Use Committee approved all experiments, and work was completed according to guidelines of the National Institutes of Health and the Institute of Laboratory Animal Resources, National Research Council. Animals were housed in an accredited facility with 12-hour light/dark cycles and supplied food and water *ad libitum* (Pico-Lab Rodent Diet 20, LabDiet). Whole blood was collected via cardiac puncture at the time of euthanasia and serum was separated (BD Biosciences, Franklin Lakes, NJ). Serum biomarkers for bone formation (P1NP) and resorption (CTX and TRAP) were performed by ELISA per the manufacturer's instructions (Immunodiagnostic Systems, Boldon, UK).

DEXA, radiographs, and microCT

Serial in vivo DEXA scans were performed on male WT and *Girk3*$^{-/-}$ mice at 4-, 6-, 12-, and 18-weeks of age using a PIXImus2 scanner (Lunar, Madison, WI). Mice were anesthetized with isoflurane and placed on the imaging tray in a prostrate position. Whole-body scans were performed, but the skull was excluded from subsequent analyses. Following euthanasia at 24 weeks of age, the right femurs were collected, cleaned of soft tissue, fixed in 10% neutral buffered formalin overnight, and stored in 70% ethanol until analysis. Radiographs were acquired using a Faxitron X-ray imaging cabinet (Faxitron Biotopics, Tuscon, AZ). Limb length was measured on radiographs using ImageJ software (NIH, Bethesda, MD, USA; https://imagej.nih.gov/ij/). Micro-CT imaging of the right femur was then performed using a SkyScan 1276 scanner (Bruker, Kontich, Belgium). Scans were performed at 55 kV, 200 μA, 10 μm pixel resolution, 0.2° rotation steps for 360°, 4 frames average imaging with a 0.25 mm A1 filter. The acquired scans were reconstructed using the Skyscan NRecon software with beam hardening and post-alignment correction. Trabecular and cortical analyses of the femur were performed using Bruker CtAN software. The datasets were oriented in 3D to vertically align the longitudinal axis of each femur. A region of interest (ROI) for trabecular bone was defined as 5% the length of each bone, beginning 10% bone's-length distance away from the distal growth plate. A gray-value threshold of 50 was applied to trabecular segmentations. For cortical bone analyses, the ROI was defined as 5% of total femur length beginning at the femoral midpoint. A gray-value threshold of 90 was applied to cortical segmentations.

Cortical bone density was measured at distinct densities by multilevel Otsu thresholding as described.[31,32] Briefly, automated thresholding was performed on the cortical ROI of WT samples. The density thresholds were recorded and averaged to calculate the final thresholds into which all samples were segmented. The amount of bone tissue (Bone Area (mm^2) or Bone Area / Tissue Area (%)) that fell within each thresholded region was then calculated. Threshold values were converted to mgHA/cm^3 after calibrating against the phantoms.

Three-point bend testing

Left femora were collected and stored in saline-soaked sterile gauze at –20°C until the time of testing. Bones were thawed and measured with a digital caliper (Digimatic Absolute, Mitutoyo, Aurora, IL) capturing the total length of the femur, the medial–lateral diameter at the mid-shaft and the anterior–posterior dimension at the mid-shaft. A 3-point bend fixture was mounted on a servohydraulic mechanical testing frame (Model 858, MTS Systems, Eden Prairie, MN) instrumented with a 25-lb capacity load cell (Model MDB-25, Transducer Techniques, Temecula, CA). Femurs were mounted on supports spanning 8 mm. Point loading was applied to the femur midshaft allowing the bones to flex about an axis aligned with the medial–lateral line. Specimens were kept moist by irrigating them with phosphate buffered saline solution. Loading was applied under displacement control at a rate of 20 mm/min until fracture. Force and displacement data was sampled at 256 Hz. The peak load and peak displacement were quantified. The stiffness was calculated from the slope of the linear region of the force displacement curve.

Histomorphometry

For histomorphometry studies, tibiae (*Girk3*$^{fl/fl}$ and *Girk3*-CKO$_{2.3Col1a1}$) or femurs (WT and *Girk3*$^{-/-}$) were decalcified in 15% EDTA for 14 days and subjected to paraffin embedding and longitudinal sectioning. Sections were either stained with hematoxylin and eosin and mounted with a xylene-based mounting medium to visualize osteoblasts or stained with a tartrate-resistant acid phosphatase (TRAP) / fast green protocol and mounted with an aqueous mounting medium to visualize osteoclasts. Histological images in the secondary spongiosa were captured using a Zeiss Axioscanner slide scanner with a 20X objective. Osteoblast number (N.Ob/B.Pm, #/mm), osteoblast surface (Ob.S/BS, %), osteoclast number (N.Oc/BS, #/mm), and osteoclast surface (Oc.S/BS, %)

measurements were quantified using Bioquant Osteo software (Bioquant Osteo, Nashville, TN) as previously described.[33]

Calvarial osteoblast culture

Calvarial osteoblasts were isolated from 2- to 3-day-old WT and *Girk3*$^{-/-}$ littermates as described.[30,34] Briefly, parietal and frontal bones were dissected from 2- to 3-day-old pups, cleaned of soft tissues, rinsed with PBS, minced, and digested in medium (alpha-MEM) containing collagenase and trypsin while mixing on an orbital shaker at 37°C. After 20 minutes, bone chips were vortexed, medium was aspirated, and fresh digestion medium was replaced for an additional hour. Collagenase digestion was repeated twice. Following the final digestion, the supernatant and bone chips were plated and expanded in growth medium (alpha-MEM containing 10% FBS and 1% penicillin–streptomycin). Once 70–80% confluent, cells were trypsinized and plated at 1 x 10^5 cells / well in 6-well plates, then grown to 90–95% confluence, at which time growth medium was replaced with osteogenic differentiation medium (alpha-MEM containing 10% FBS, 1% Pen-Strep, 0.05 mg/mL ascorbic acid, and 10 mM β-glycerophosphate). Alkaline phosphatase and alizarin red staining were performed on days 10 and 28 of osteogenic culture, respectively. RNA was collected in Trizol on days 7, 14, and 21 of osteogenic culture. All in vitro experiments were repeated in at least 3 independent experiments with at least 1 biological replicate per experiment. Representative results are shown.

Bone marrow stromal cell culture

Bone marrow stromal cells (BMSCs) were isolated from 4- or 24-week-old male mice as previously described.[35,36] Briefly, bone marrow was isolated via centrifugation from the iliac bones, femurs, and tibiae. For proliferation assays, cells were maintained in growth medium and plated as described in specific methods below. For differentiation assays, cells were seeded at 1 x 10^5 cells/cm^2 in 12-well plates and grown to 90–95% confluence. Differentiation medium was then applied to induce osteogenic differentiation. In some experiments, 50 ng/mL DKK-1 (R&D Systems, Minneapolis, MN, USA) or 3 μM XAV939 (Selleck Chemicals, Houston, TX, USA) were also added as indicated. Crystal violet, alkaline phosphatase, and alizarin red staining was performed at the times indicated in each experiment. RNA was collected on days 4 and 21 of osteogenic culture. All in vitro experiments were repeated in at least 3 independent experiments with at least 1 biological replicate per experiment. Representative results are shown.

Cell metabolic activity assays and live cell imaging

Bone marrow stromal cells were seeded at 3 x 10^4 cells/cm^2 in 96-well flat-bottom plates and allowed to adhere overnight. MTS assays were performed per the manufacturer's instructions (Promega, Madison, WI, USA) and measured via spectrophotometer 4 hours after addition of the MTS reagent. For live-cell imaging, cell confluency was detected in real-time with the IncuCyte S3 Live Cell Analysis System (Roche Applied Science, Indianapolis, IN, USA), with 4 captures per well every hour for up to 96 hours. All in vitro experiments were repeated in at least 3 independent experiments with at least 1 biological replicate per experiment. Representative results are shown.

RNA-sequencing (RNA-seq) and pathway analysis

RNA was isolated from flushed long bones of male 24-week-old WT and *Girk3*$^{-/-}$ mice ($n = 4$) and submitted to Genewiz (Azenta Life Sciences, Plainfield, NJ) for bulk next generation RNA-sequencing. RNA Sequencing libraries were prepared using the NEBNext Ultra II RNA Library Prep Kit for Illumina per the manufacturer's instructions (NEB, Ipswich, MA). Samples were sequenced on an Illumina instrument (4000 or equivalent) using a 2 x 150 bp paired end (PE) configuration. Image analysis and base calling were conducted by the Control software. Raw sequence data (.bcl files) generated by the sequencer were converted into fastq files and de-multiplexed using Illumina's bcl2fastq 2.17 software. One mismatch was allowed for index sequence identification. Trimmed reads were then mapped to the reference genome available on ENSEMBL using the STAR aligner v.2.5.2b. Unique gene hit counts were calculated by using feature Counts from the Subread package v.1.5.2. Only unique reads that fell within exon regions were counted.

After extraction of gene hit counts, the gene hit counts table was used for downstream differential expression analysis. Using DESeq2, a comparison of gene expression between the groups of samples was performed. The Wald test was used to generate p-values and Log2 fold changes. Genes with adjusted p-values<0.05 and absolute log2 fold changes >1 were considered differentially expressed genes for each comparison. A gene ontology analysis was performed on the statistically significant set of genes. Gene expression data were submitted to the Gene Expression Omnibus database (accession number GSE264200).

RNA extraction and qRT-PCR

Cells from BMSC and calvarial cultures were washed with PBS, then mechanically disrupted using a cell scraper in 1 mL of TRIzol (Invitrogen). Total RNA was extracted using an RNA purification kit (Zymo Research) and 1.5–2 μg (depending on the experiment) was reverse transcribed to cDNA with the iScript cDNA synthesis kit (BioRad). Quantitative RT-PCR was completed using gene-specific primers for *Alpl* (5'-GAACAGACCCTCCCCACGAG-3', 5'-GTGCCGATGGCCAGTACTAA-3'), *Bglap* (5'- TTCTGCTCACTCTGCTGACC-3', 5'-TTAAGCTCACACTGCTCCCG-3'), *Ibsp* (5'-AACAATCCGTGCCACTCACT-3', 5'-GGCCGGTACTTAAAGACCCC-3'), *Sfrp3* (5'-CAAGGGACACCGTCAATCTT-3', 5'-CATATCCCAGCGCTTGACTT-3'), *Sfrp4* (5'-CCCTCGAACACAAGTCCCTC-3', 5'-AGCATCATCCTTGAACGCCA-3'), *Sfrp5* (5'-CTGGACAACGACCTCTGCAT-3', 5'-TCGGTCCCCGTTGTCTATCT-3') Transcript levels were normalized to the reference gene *Ywhaz* (5'-GCCCTAAATGGTCTGTCACC-3', 5'-GCTTTGGGTGTGACTTAGCC-3'). Abundance and relative fold changes in transcript gene expression were quantified using the $2^{-\Delta\Delta Ct}$ method relative to WT cells.[37]

Statistics

Statistics were performed in GraphPad Prism (Version 9) using Student's t-test or 2-way ANOVA as appropriate with repeated measures and post hoc tests for multiple comparisons where necessary. Specific statistical tests are detailed in each experiment. Outliers were identified by Grubbs' tests and removed where necessary. Data are depicted as box and whisker plots or means ± standard deviation with individual points shown.

Table 1. MicroCT and histomorphometry parameters of 24-week-old male WT and *Girk3*$^{-/-}$ mice.

Output	Mean ± SD		
ELISA	**WT ($n = 8$)**	***Girk3*$^{-/-}$ ($n = 10$)**	***p*-Value**
P1NP (ng/mL)	36.0 ± 11.3	28.8 ± 9.2	0.15
CTX (ng/mL)	23.9 ± 6.0	24.6 ± 5.2	0.79
Trabecular microCT			
Bone volume fraction (%)	16.1 ± 3.7	21.9 ± 6.7	*0.04*
Bone mineral density (mg/cm^3)	126 ± 22	155 ± 22	*0.01*
Trabecular number (mm^{-1})	1.89 ± 0.23	2.35 ± 0.51	*0.03*
Trabecular thickness (μm)	85 ± 14	92 ± 10	0.21
Trabecular spacing (μm)	235 ± 19	215 ± 33	0.14
Cortical microCT			
Bone area (mm^2)	0.86 ± 0.04	0.88 ± 0.07	0.43
Tissue area (mm^2)	1.84 ± 0.07	1.87 ± 0.18	0.69
Bone area fraction (%)	46.8 ± 0.9	47.4 ± 1.4	0.28
Cortical thickness (μm)	186 ± 6.3	190 ± 7.0	0.36
Periosteal perimeter (mm)	5.29 ± 0.11	5.33 ± 0.24	0.71
Endosteal perimeter (mm)	3.94 ± 0.09	4.00 ± 0.31	0.63
Tissue mineral density (g/cm^3)	1.12 ± 0.04	1.12 ± 0.04	0.71
Mean polar moment of inertia (mm^4)	0.41 ± 0.04	0.43 ± 0.08	0.58
Histomorphometry			
Number of osteoblasts	70 ± 41	98 ± 71	0.36
Bone surface (μm)	13.9 ± 5.0	14.6 ± 7.2	0.82
Number of osteoblasts / bone surface (1/μm)	4.9 ± 2.6	6.9 ± 2.6	0.13
Osteoid surface (μm)	1.1 ± 0.7	1.6 ± 1.2	0.39
Osteoid surface / bone surface (%)	0.08 ± 0.05	0.11 ± 0.05	0.18
Number of osteoclasts	35.6 ± 25.8	14.3 ± 9.3	0.15
Number of osteoclasts / bone surface (1/μm)	4.1 ± 1.9	3.1 ± 1.6	0.39
Osteoclast surface (μm)	0.80 ± 0.61	0.25 ± 0.20	0.12
Osteoclast surface / bone surface (%)	0.09 ± 0.05	0.05 ± 0.02	0.11

P-values <0.05 are italicized.

Results

Girk3 deletion increases bone mass in 24-week-old male mice

We previously showed that WT and *Girk3*$^{-/-}$ littermates have equivalent bone mass at 4 weeks of age.[23] Serial DEXA scanning of mice at 4, 6, 12, and 18 weeks of age revealed that BMD was not different between the groups at 4, 6, or 12 weeks of age, while modest but non-significant increases appeared in *Girk3*$^{-/-}$ mice at 18 weeks (Figure 1A). By 24 weeks of age, trabecular bone volume fraction at the distal femur (Figure 1B and C, Table 1) was significantly elevated in *Girk3*$^{-/-}$ mice. Trabecular BMD (Figure 1D) and trabecular number (Figure 1E) were also higher in *Girk3*$^{-/-}$ mice. No changes in the cortical bone parameters or strength properties were detected (Table 1, Supplementary Table 1). Osteoclast number, osteoclast surface, and osteoclast surface per bone surface were slightly but non-significantly lower in *Girk3*$^{-/-}$ compared to WT mice (Table 1). There were no differences in bone surface, osteoid surface, or number of osteoblasts. A slightly greater number of osteoblasts per bone surface and osteoid surface per bone surface were observed in *Girk3*$^{-/-}$ compared to WT mice (Table 1).

BMSCs from *Girk3*-/- mice have accelerated proliferation, metabolic activity, and mineralization in vitro

As osteoblast activity was mildly increased in *Girk3*$^{-/-}$ mice in vivo, we next sought to understand the high bone mass phenotype in *Girk3*$^{-/-}$ animals by examining the osteogenic potential of *Girk3*$^{-/-}$ cells in vitro. After 21 days in growth medium, *Girk3*$^{-/-}$ BMSCs had greater crystal violet staining, indicating increased cell number (Figure 2A). Tracking the confluence of BMSCs isolated from 4-week-old male WT and *Girk3*$^{-/-}$ mice in a live cell assay also demonstrated greater proliferative capacity in *Girk3*$^{-/-}$ BMSCs (Figure 2B). Elevated proliferation was particularly evident early in culture, as there was a 6% increase in cell confluence in *Girk3*$^{-/-}$ compared to WT mice in the first 2 hours of the experiment (Figure 2C). Cell metabolic activity, as determined by MTS assay, was also elevated in *Girk3*$^{-/-}$ compared to WT BMSCs (Figure 2D).

Girk3$^{-/-}$ BMSCs from 24-week-old mice cultured in osteogenic medium produced more alkaline phosphatase after 7 days compared to WT littermates (Figure 2E). After 12 days in osteogenic medium, calcification was evident only in *Girk3*$^{-/-}$ BMSCs, demonstrating that mineralization was accelerated (Figure 2F). By day 21 in osteogenic medium, both WT and *Girk3*$^{-/-}$ BMSCs were mineralized, with more calcification evident in the *Girk3*$^{-/-}$ cells (Figure 2G). On day 21 of osteogenic culture, BMSCs from *Girk3*$^{-/-}$ mice had greater expression of osteocalcin and bone sialoprotein than WT littermates (Figure 2H). Mineralization was also accelerated in calvarial osteoblasts isolated from 2- to 3-day-old *Girk3*$^{-/-}$ mice. Like the BMSCs from adult mice, *Girk3*$^{-/-}$ calvarial osteoblasts had accelerated mineralization as indicated by increased alkaline phosphatase deposition (Supplementary Figure 1A) on day 10 in culture and extracellular matrix deposition on day 28 in culture as compared to WT calvarial osteoblasts (Supplementary Figure 1B). Calvarial osteoblasts from *Girk3*$^{-/-}$ mice also produced more alkaline phosphatase (Supplementary Figure 1C) and osteocalcin (Supplementary Figure 1D) mRNA transcripts than WT cells throughout osteogenic culture.

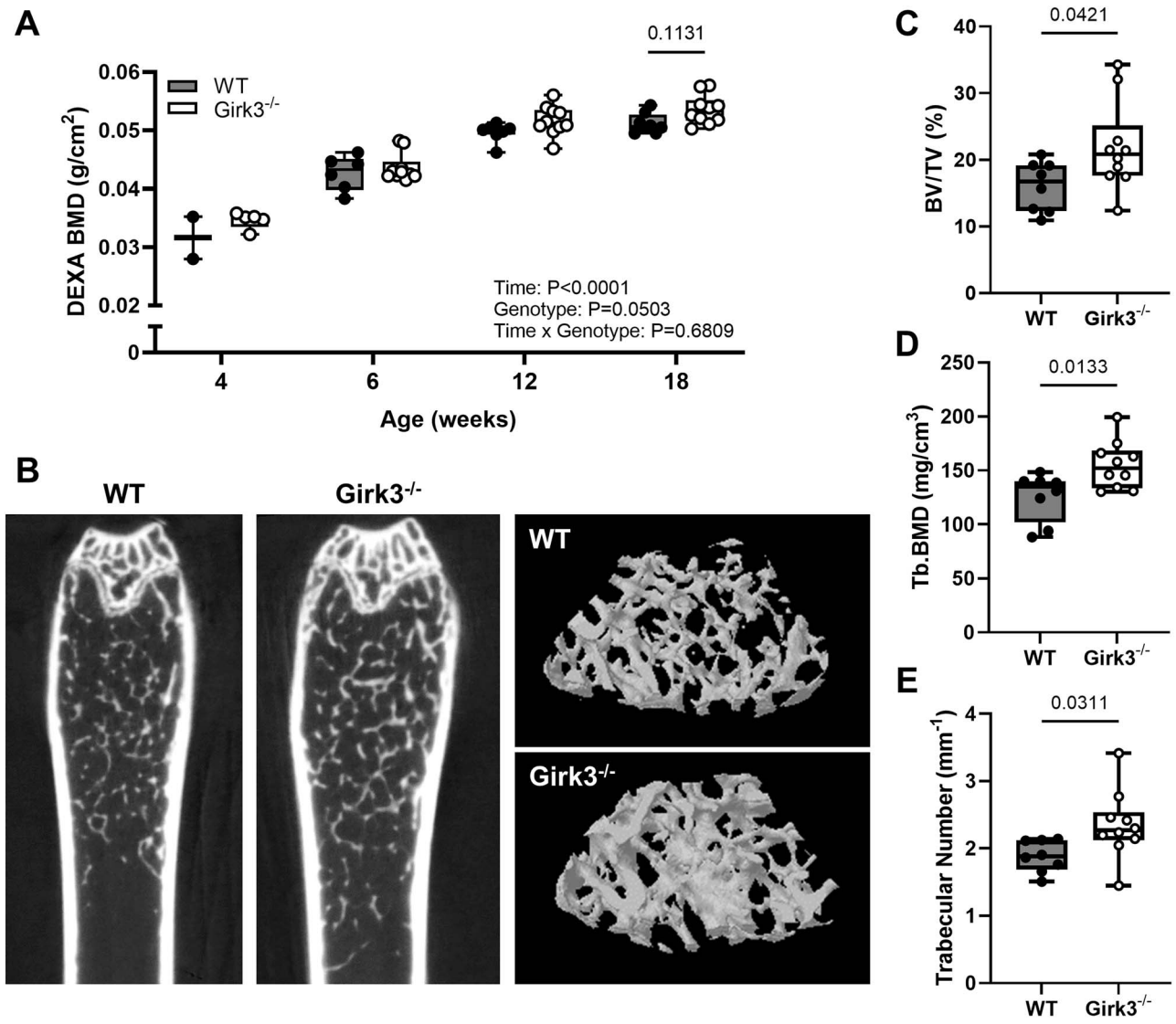

Figure 1. *Girk3* deletion increases trabecular bone mass in 24-week-old male mice. (A) Bone mineral density was determined by DEXA scanning at 4, 6, 12, and 18 weeks of age. (B) MicroCT reconstructions of distal femora of 24-week-old mice. (C) Bone volume fraction (bone volume / tissue volume; BV/TV) of distal femora. (D) Trabecular BMD of distal femora. (E) Trabecular number of distal femora. Statistics were performed using a 2-way ANOVA with repeated measures with Šídák's multiple comparisons or students *t*-test. Data are shown as box plots from the 25th to 75th percentiles, with whiskers extending to the minimum and maximum value.

Enhanced osteogenesis in *Girk3*$^{-/-}$ cells is dependent on Wnt signaling

To determine the mechanisms underlying enhanced mineralization in *Girk3*$^{-/-}$ mice, diaphyseal femoral bone tissue (flushed of marrow) from 24-week-old WT and *Girk3*$^{-/-}$ mice were submitted for bulk RNA-Sequencing and bioinformatic analysis. About 45 genes were more highly expressed in *Girk3*$^{-/-}$ bone, while 60 genes were repressed ($p_{adj} \leq 0.05$, log2 fold change ≥ 1) (Supplementary Table 2). "Canonical Wnt signaling (GO:0060070)" was among the top differentially regulated GO terms in *Girk3*$^{-/-}$ bone (Figure 3A) and included transcripts such as *Wnt6* and *Sfrp5*.

In vitro, BMSCs from 24-week-old *Girk3*$^{-/-}$ mice had altered expression of Wnt-regulating genes, including higher expression of pro-osteogenic *Sfrp3* (Figure 3B) and lower expression of Wnt-antagonizing *Sfrp4* and *Sfrp5* (Figure 3C) on day 4 in culture. Neither of the Wnt inhibitors Dkk1 nor XAV939 affected proliferation in *Girk3*$^{-/-}$ BMSCs, as measured by live cell proliferation assays (Supplementary Figure 2A and B) and MTS assays (Supplementary Figure 2C). Both Wnt inhibitors repressed osteoblast maturation in both WT and *Girk3*$^{-/-}$ BMSCs, as indicated by lower alkaline phosphatase (Figure 3D) and Alizarin red staining (Figure 3E and F).

Conditional deletion of *Girk3* in osteoblasts is sufficient to induce high trabecular and cortical bone mass at 24 weeks of age in male mice

To determine if *Girk3* deletion in osteoblasts is sufficient to recapitulate the high bone mass phenotype observed in *Girk3*$^{-/-}$ mice, we generated mice with a conditional deletion for *Girk3* using a Cre-recombinase driven by the 2.3 kb-Col1a1 promoter.[28] At 4 weeks of age, there

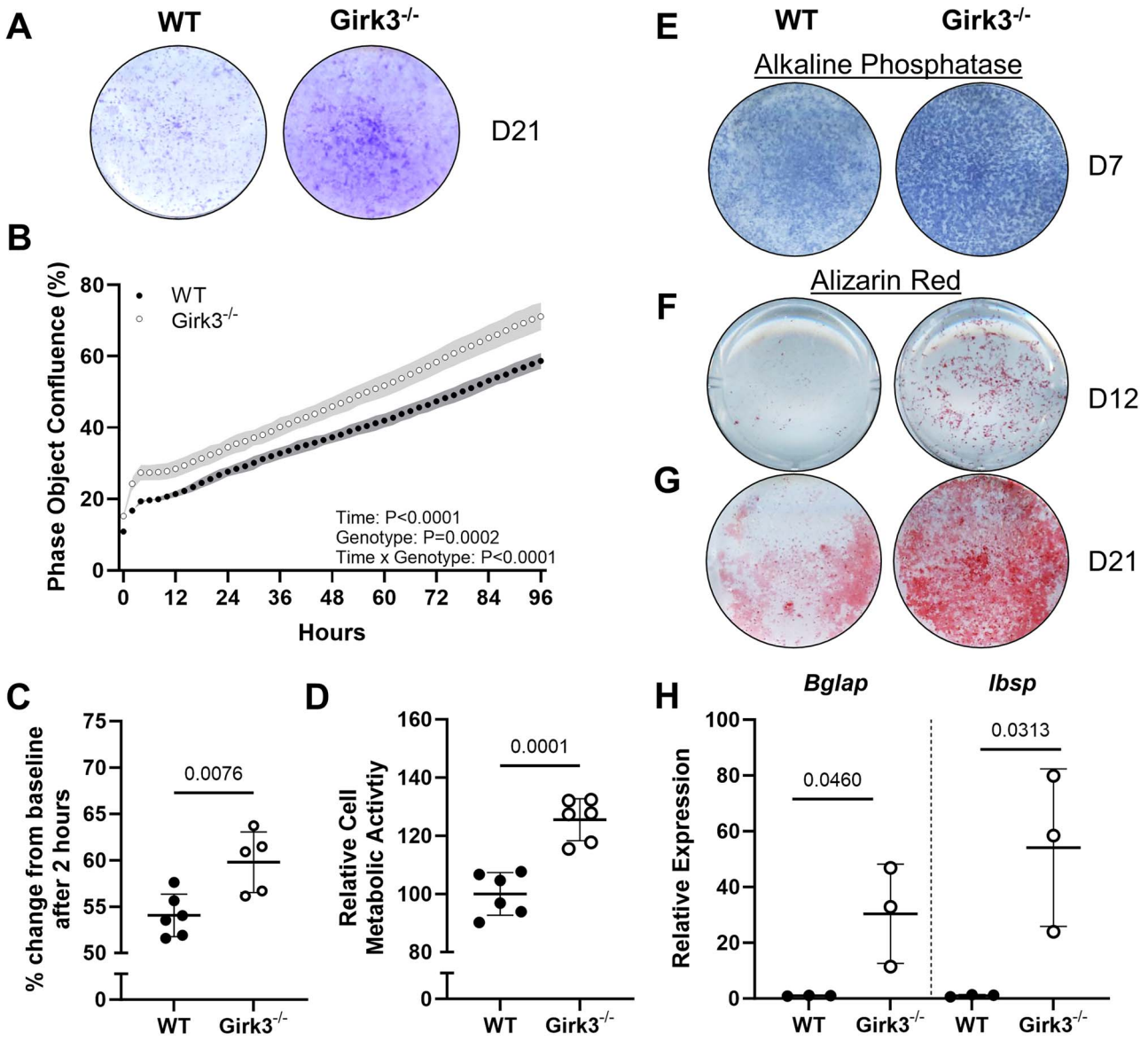

Figure 2. *Girk3* deletion increases in vitro proliferation and osteogenesis. (A) BMSCs were isolated from the iliac bones, femur, and tibiae of 24-week-old male WT and *Girk3*$^{-/-}$ mice and placed into growth medium. After 21 days, crystal violet staining was performed. (B) BMSCs were isolated from 4-week-old male WT and *Girk3*$^{-/-}$ mice and placed into growth medium in a live cell tracker. Percent confluence of the plate was monitored ($n = 6$ wells per genotype) for 96 hours. (C) The percent change from baseline was calculated for the first 2 hours of growth. (D) Cell metabolic activity as evaluated by MTS assay was measured in 4-week-old WT and *Girk3*$^{-/-}$ BMSCs 4 hours after adding the MTS reagent. (E–H) BMSCs isolated from 24-week-old male WT and *Girk3*$^{-/-}$ mice were isolated and placed into osteogenic medium. (E) Alkaline phosphatase staining was performed on day 7 in osteogenic culture. Alizarin red staining was performed on day 12 (F) and day 21 (G) of osteogenic culture. (H) Transcript levels of osteocalcin (*Bglap*) and bone sialoprotein (*Ibsp*) were evaluated in the BMSCs cultured in osteogenic medium for 21 days via qRT-PCR. Statistics were performed using a 2-way ANOVA with Šídák's post-hoc tests or Student's *t*-test. Data are shown as mean ± standard deviation.

was no difference in the trabecular bone of male *Girk3*-CKO$_{2.3Col1a1}$ mice compared to littermate controls and there was less cortical bone (Supplementary Table 3). By 24 weeks of age, male *Girk3*-CKO$_{2.3Col1a1}$ mice had increased trabecular bone mass (Figure 4A). Consistent with 24-week-old *Girk3*$^{-/-}$ mice, male *Girk3*-CKO$_{2.3Col1a1}$ mice had increased bone volume fraction (Figure 4B), moderately increased trabecular BMD (Figure 4C), and a greater number of trabeculae (Figure 4D) compared to controls at 24 weeks of age. *Girk3*-CKO$_{2.3Col1a1}$ mice also had reduced trabecular spacing compared to controls (Figure 4E). Histomorphometry revealed a greater number of osteoblasts on trabecular bone surfaces (Figure 4F and G), reflecting both an increased number of osteoblasts and increased bone surface in *Girk3*-CKO$_{2.3Col1a1}$ compared to *Girk3*$^{fl/fl}$ mice. *Girk3*-CKO$_{2.3Col1a1}$ mice also had a greater osteoid surface, resulting in moderately increased osteoid surface per bone surface (Figure 4H, Table 2).

The cortical bone of 24-week-old male mice was also altered by deletion of *Girk3* in mature osteoblasts (Figure 5A, Table 2). While cortical TMD was decreased (Figure 5B), cortical thickness was increased in *Girk3*-CKO$_{2.3Col1a1}$ mice compared to littermate controls (Figure 5C). The increased thickness of the cortical bone was due to a larger periosteal perimeter in *Girk3*-CKO$_{2.3Col1a1}$ mice (Figure 5D); the endosteal perimeter was unchanged (Figure 5E). MicroCT analysis also revealed that 24-week-old male *Girk3*-CKO$_{2.3Col1a1}$ mice had a greater mean polar moment

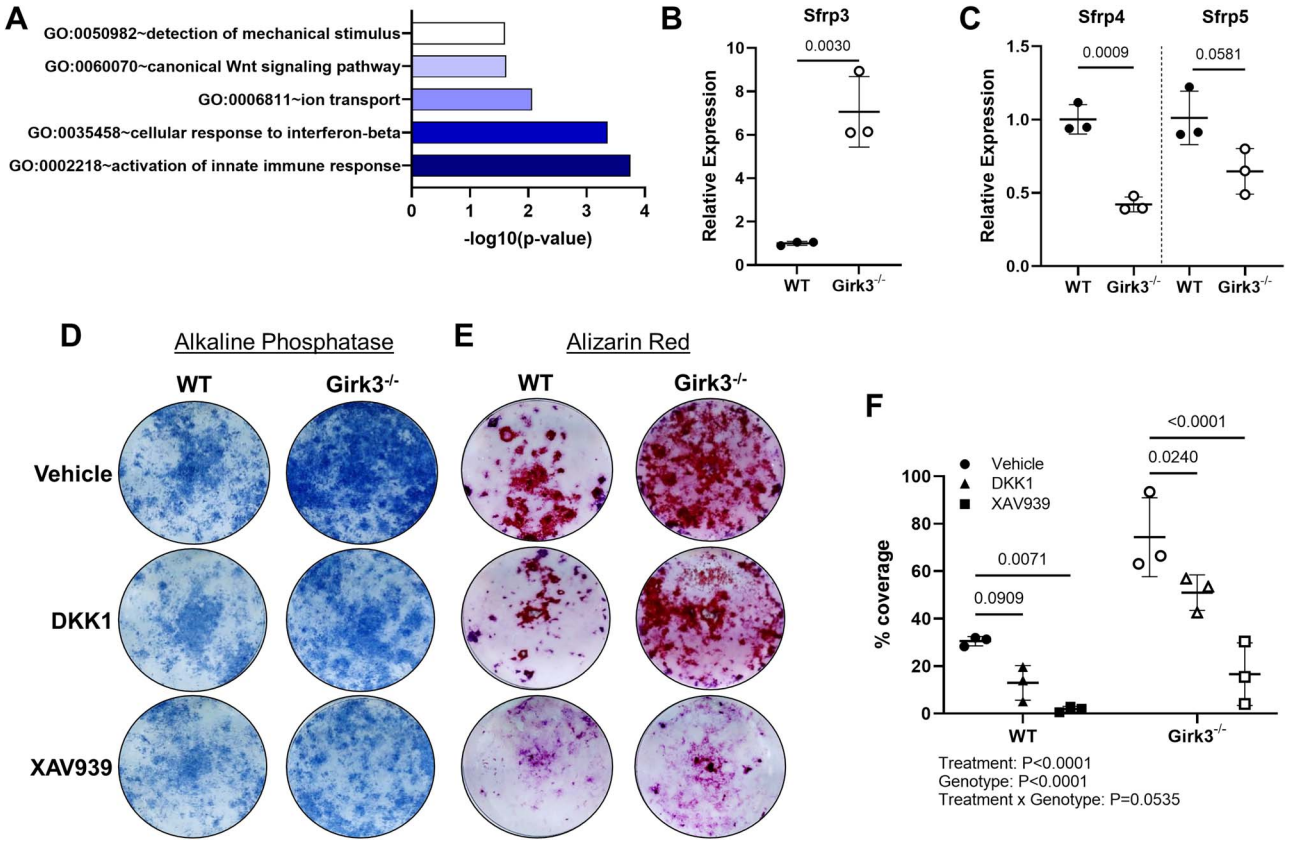

Figure 3. Increased osteogenesis in *Girk3*$^{-/-}$ BMSCs is dependent on Wnt signaling. (A) Bulk RNA-sequencing was performed on flushed diaphyseal femoral bone from 24-week-old WT and *Girk3*$^{-/-}$ mice and GO-term analysis was performed. Subsequent qRT-PCR on BMSCs from 24-week-old WT and *Girk3*$^{-/-}$ mice cultured in osteogenic medium for 4 days showed (B) increased expression of *Sfrp3* and (C) decreased expression of *Sfrp4* and *Sfrp5*. (D, E) BMSCs from 24-week-old WT and *Girk3*$^{-/-}$ mice were placed in osteogenic medium containing Dkk1 (50 ng/mL), XAV939 (3 μM), or vehicle (0.1% BSA in PBS). Alkaline phosphatase (D4) (D) and Alizarin red (D12) staining (E) was performed and quantified (F). Statistics were performed using Student's *t*-test or a 2-way ANOVA with Šídák's post hoc tests. Data are shown as mean ± standard deviation.

of inertia (Figure 5F) and could withstand a greater maximum load (Figure 5G) with a greater energy to failure (Figure 5H) in 3-point bend testing (Supplementary Table 4).

We next sought to further define the cortical TMD in *Girk3*-CKO$_{2.3Col1a1}$ mice by thresholding the bone into low, medium, and high densities (Figure 6A).[31,32] Bone area of low- and medium-density bone was increased in *Girk3*-CKO$_{2.3Col1a1}$ mice, but there was no change in the bone area of high-density bone, compared to *Girk3*$^{fl/fl}$ animals (Figure 6B–D). After normalizing bone area to total tissue area, *Girk3*-CKO$_{2.3Col1a1}$ mice had a greater proportion of mid-density bone compared to *Girk3*$^{fl/fl}$ littermates (Figure 6E–G). Bone strength correlates with parameters detectable by microCT, including mean polar moment of inertia.[38] We confirmed that mean polar moment of inertia correlated with maximum load in our samples (Supplementary Figure 3). Low-density (Figure 6H) and medium-density (Figure 6I), but not high-density (Figure 6J), bone area were positively correlated with maximum load withstood by the mid-diaphyseal bone in 3-point bend testing.

Discussion

In adult vertebrates, bone tissue is maintained by a balance of formation and resorption and regulated by a host of signaling pathways, hormones, and mechanical forces. During aging, bone mass declines in men by 1% each year after the age of 30.[5] Age-related declines in bone mass are due to increased bone resorption and reduced bone formation, in part due to declining progenitor cell numbers.[3] Adult bone accrual has been demonstrated in few mouse models, including a transgenic mouse model of suppressed $G_{i/o}$ signaling.[6,7] In this project, we describe the GPCR-$G_{i/o}$ coupled K^+ ion channel subunit GIRK3 as a novel regulator of bone mass in mature skeletal tissue. We previously found that *Girk3* negatively regulates bone lengthening through 12 weeks of age in mice. Herein, we report that *Girk3* suppresses bone mass accrual after 18 weeks of age. By 24-weeks-old, male *Girk3*$^{-/-}$ mice have more trabeculae in long bones and greater trabecular bone mass than WT mice. BMSCs from *Girk3*$^{-/-}$ mice have higher proliferation rates and cell metabolic activity, as well as increased mineralization capacity in vitro, at least in part due to activated Wnt signaling. Conditional deletion of *Girk3* in osteoblasts is sufficient to induce high bone mass in both cortical and trabecular compartments of 24-week-old male mice. Female *Girk3*$^{-/-}$ mice were also evaluated and are the subject of a separate analysis because they exhibit systemic mechanisms of action that are distinct from male mice.

Deletion of *Girk3* causes late onset increases in bone mass, beginning at approximately 18 weeks of age. In C57BL/6 mouse models, peak bone mass is achieved by approximately 24 weeks of age, although this is highly dependent on the substrain, sex, skeletal compartment, and method of

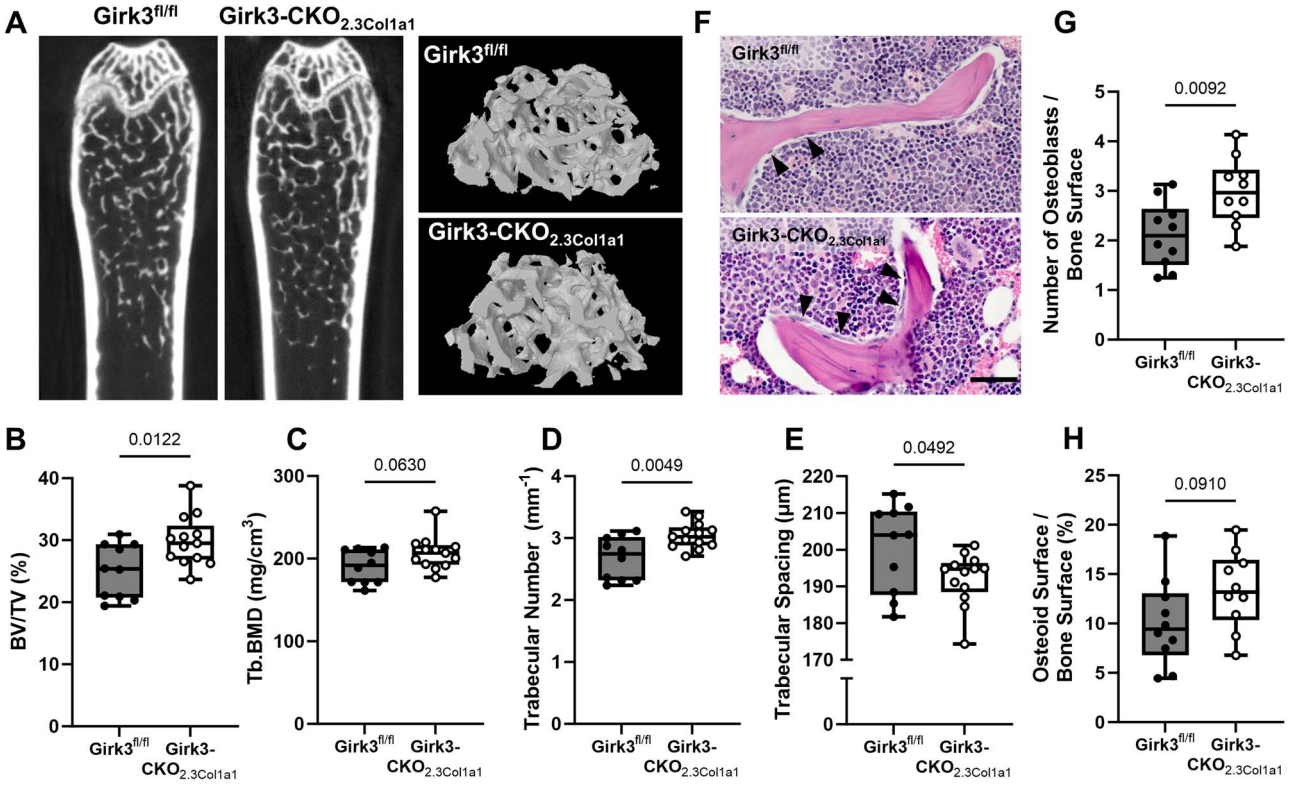

Figure 4. Conditional *Girk3* deletion in osteoblasts increases trabecular bone mass in 24-week-old male mice. (A) MicroCT reconstructions of distal femora. (B–E) Bone volume fraction (bone volume / tissue volume; BV/TV) (B), trabecular BMD (C), trabecular number (D), and trabecular spacing (E) of the distal femora. (F) Histomorphometry of proximal tibia of control and *Girk3*-CKO$_{Col1a1}$ mice. (G) The number of osteoblasts per bone surface. (H) The osteoid surface per bone surface. Statistics were performed using students *t*-test. Data are shown as box plots from the 25th to 75th percentiles, with whiskers extending to the minimum and maximum value and means shown by horizontal lines.

Table 2. MicroCT and histomorphometry parameters of 24-week-old male *Girk3*$^{fl/fl}$ and *Girk3*-CKO$_{2.3Col1a1}$ mice.

Output	Mean ± SD		
Body measurements	***Girk3*$^{fl/fl}$ ($n = 10$)**	***Girk3*-CKO$_{2.3Col1a1}$ ($n = 13$)**	***p*-Value**
Body weight (g)	36.7 ± 3.9	35.8 ± 4.0	0.62
Femur length (cm)	1.40 ± 0.01	1.39 ± 0.03	0.68
ELISA			
P1NP (ng/mL)	3.5 ± 0.6	3.6 ± 0.8	0.82
TRAP (ng/mL)	7.9 ± 1.5	7.4 ± 2.1	0.54
Trabecular microCT			
Bone volume fraction (%)	25.1 ± 4.4	29.9 ± 4.0	*0.01*
Bone mineral density (mg/cm^3)	190 ± 20	207 ± 20	*0.06*
Trabecular number (mm^{-1})	2.68 ± 0.34	3.04 ± 0.21	*0.005*
Trabecular thickness (μm)	93.1 ± 5.4	98.0 ± 8.6	0.14
Trabecular spacing (μm)	201 ± 12	192 ± 7	*0.05*
Cortical microCT			
Bone area (mm^2)	0.92 ± 0.04	0.98 ± 0.03	*0.002*
Tissue area (mm^2)	1.97 ± 0.08	2.08 ± 0.08	*0.007*
Bone area fraction (%)	46.8 ± 2.0	47.1 ± 1.6	0.68
Cortical thickness (μm)	191 ± 7.6	198 ± 5.6	*0.02*
Periosteal perimeter (mm)	5.50 ± 0.12	5.67 ± 0.11	*0.003*
Endosteal perimeter (mm)	4.18 ± 0.17	4.22 ± 0.14	0.54
Tissue mineral density (g/cm^3)	1.16 ± 0.02	1.13 ± 0.02	*0.02*
Histomorphometry			
Number of osteoblasts	51.5 ± 27.2	100.3 ± 34.6	*0.003*
Bone surface (μm)	24.1 ± 9.9	32.9 ± 5.5	*0.02*
Number of osteoblasts / bone surface (1/μm)	2.1 ± 0.7	3.0 ± 0.7	*0.009*
Osteoid surface (μm)	2.5 ± 1.5	4.5 ± 1.9	*0.02*
Osteoid surface / bone surface (%)	10.1 ± 4.4	13.4 ± 3.9	0.09

P values less than 0.05 are italicized.

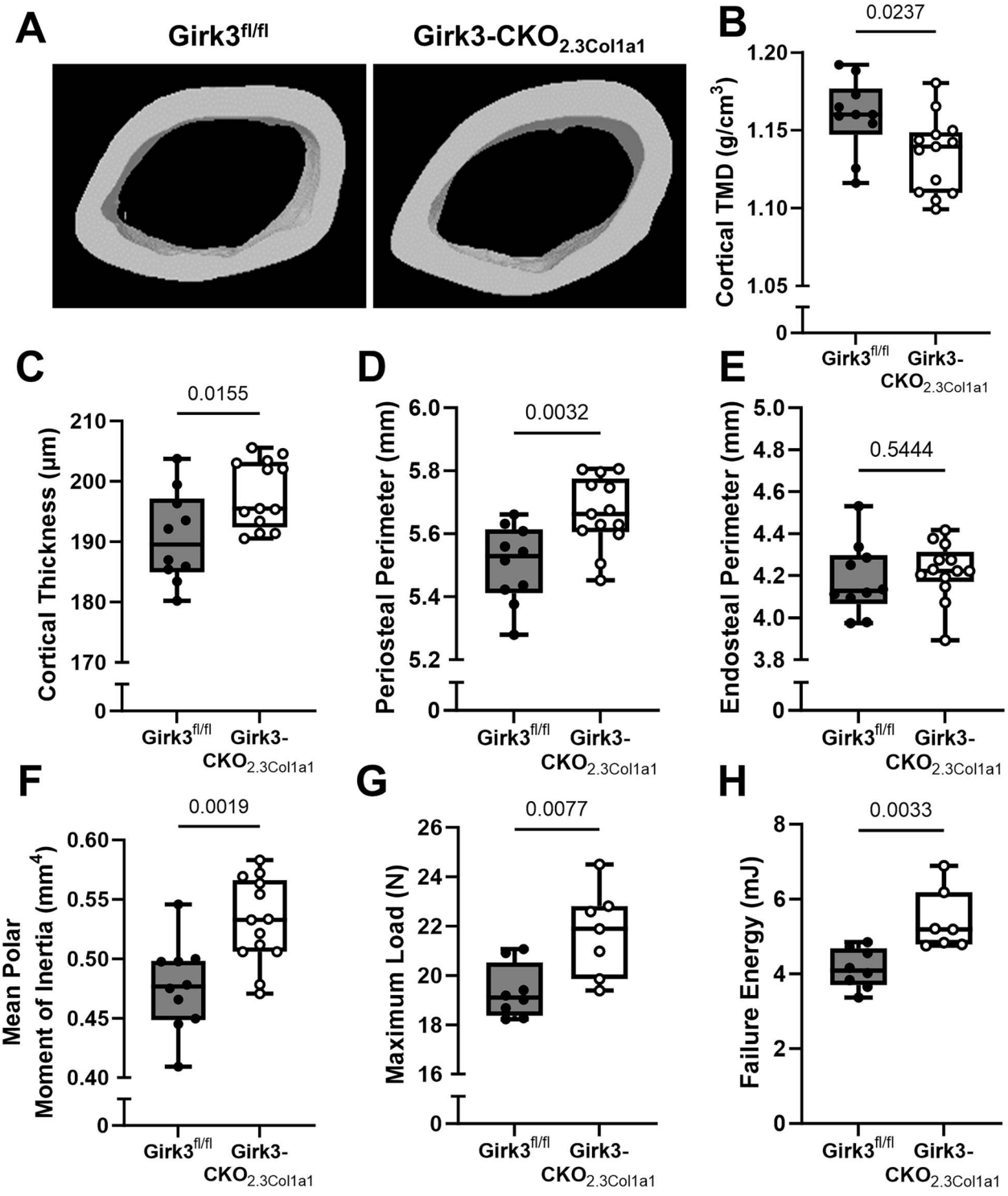

Figure 5. Conditional *Girk3* deletion in osteoblasts increases cortical bone mass and bone strength in 24-week-old male mice. (A) MicroCT reconstructions of the mid-diaphyseal femora from *Girk3*-CKO$_{2.3Col1a1}$ mice and *Girk3*$^{fl/fl}$ littermates. (B) Cortical tissue mineral density (TMD), (C) Cortical thickness, (D) periosteal perimeter, (E) endosteal perimeter, and (F) mean polar moment of inertia of the mid-diaphyseal femora. (G, H) Three-point bend testing was conducted on the femur and maximum load (G), and failure energy (H) were determined. Statistics were performed using students *t*-test. Data are shown as box plots from the 25th to 75th percentiles, with whiskers extending to the minimum and maximum value and means shown by horizontal lines.

quantification (i.e., histomorphometry, DEXA, or microCT).[39] While GIRK channels are well-characterized in excitable cells, there is a paucity of information on their role in non-excitable cells.[16] Deletion of *Girk4* reduced energy expenditure and late-onset obesity, which becomes evident at approximately 6 months of age. The authors of this study attributed the late-onset changes in energy expenditure to changing *Girk4* expression in the hypothalamus.[17] Deletion of *Girk2* in a subset of hypothalamic neurons also increased adiposity and body weight, but only after 16 weeks of age.[19] *Girk3* is

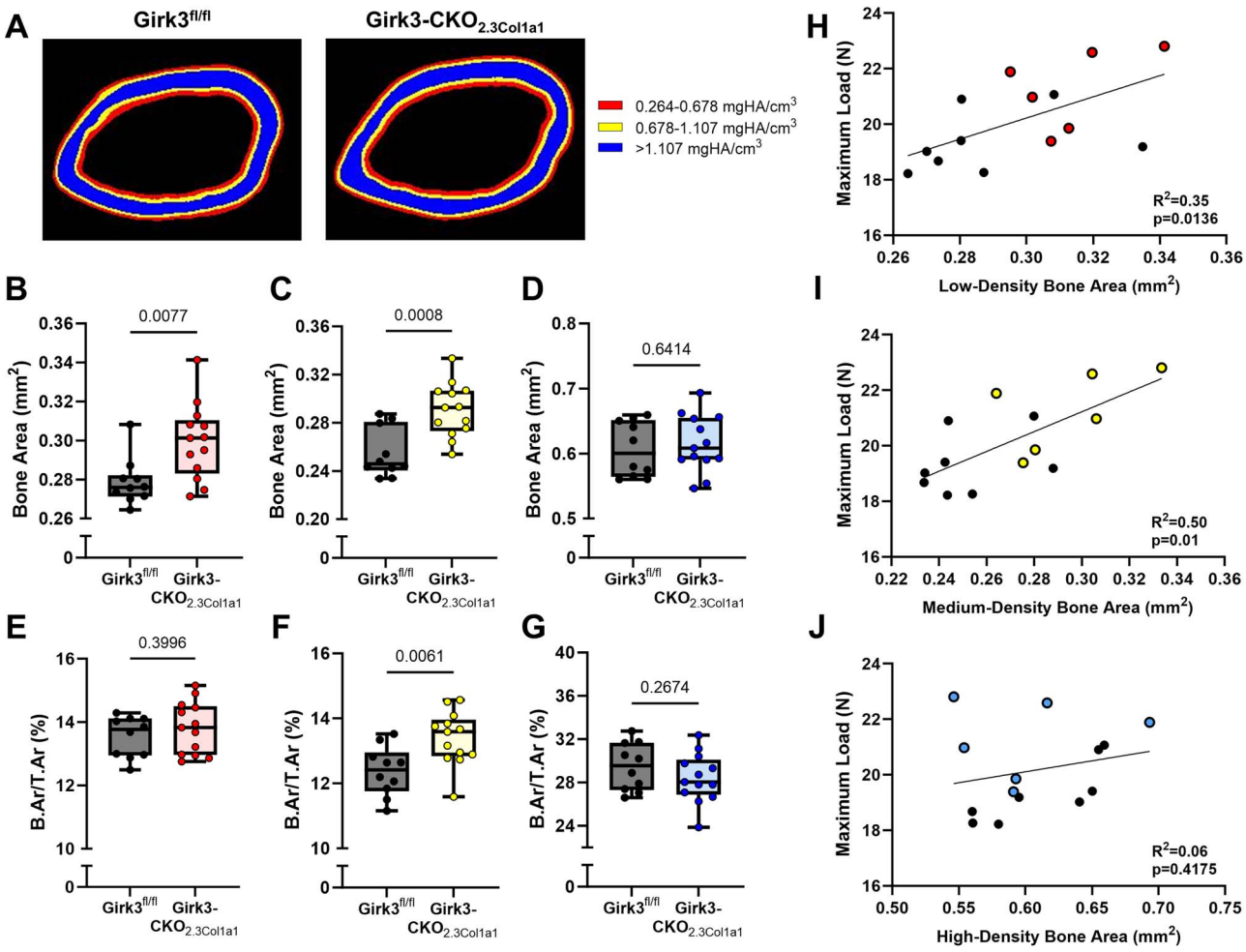

Figure 6. Conditional *Girk3* deletion in osteoblasts increases low- and medium-density cortical bone in 24-week-old male mice. (A) MicroCT reconstructions showing low, medium, and high density bone in the mid-diaphyseal femora from *Girk3*-CKO$_{2.3Col1a1}$ mice and *Girk3*$^{fl/fl}$ littermates. (B–D) Bone area thresholded by low (B), medium (C), and high (D) density. (E–G) Bone area fraction thresholded by low (E), medium (F), and high (G) density. (H–J) Correlations between maximum load in 3-point bending of the mid-diaphysis and low (H), medium (I), and high (J) density bone area. *Girk3*$^{fl/fl}$ controls are shown in closed circles and *Girk3*-CKO$_{2.3Col1a1}$ animals are shown in open circles. Statistics were performed using students *t*-test or Spearman correlation tests followed by simple linear regression. Data are shown as box plots from the 25th to 75th percentiles, with whiskers extending to the minimum and maximum value and means shown by horizontal lines.

most highly expressed in the central nervous system, often in heterotetramers with *Girk2*, therefore it is possible that a similar mechanism applies to the *Girk3*-dependent phenotype seen in bone.[11,19] It is noteworthy that both the late-onset obesity and high bone mass phenotypes in *Girk2*, *Girk3*, and *Girk4* genetically modified mice occur at approximately the same time in the murine lifespan (18–24 weeks of age).

GIRK channels are effectors of pertussin toxin (PTX)-sensitive $G_{i/o}$-coupled GPCR signaling. Inhibition of $G_{i/o}$ signaling in osteoblasts through induced expression of PTX accelerates fracture healing[40] and causes an age-related increase in bone volume,[7,8] which aligns with our observations in the *Girk3*$^{-/-}$ animals. It is therefore possible that *Girk3* loss induces bone accrual through similar GPCR-$G_{i/o}$ dependent mechanisms. A limitation of these studies is that only discrete time points were chosen for endpoint analyses. Like our study, no differences in osteoblast surface per bone surface or osteoclast surface per bone surface were detected in the mouse model of inhibited $G_{i/o}$ signaling, despite elevated bone mass.[7] It is possible that robust changes in osteoblast and osteoclast number and activity or serum biomarker values were not evident in 24-week-old mice because the window of greatest activity was missed. This hypothesis is supported by the fact that RNA-Sequencing of flushed diaphyseal bone from 24-week-old WT and *Girk3*$^{-/-}$ mice did not reveal any changes in osteogenic gene expression, despite elevated bone mass. Detailed analysis of bone and serum biomarkers from *Girk3*$^{-/-}$ mice is needed at a variety of time points to precisely define the bone cell activity underlying high bone mass.

Elevated osteogenesis in *Girk3*$^{-/-}$ bone may be partially attributable to increased canonical Wnt signaling. Wnt signaling is critical for osteoblast commitment from BMSC progenitors, as well as proliferation, differentiation, matrix production, and survival.[24,25] Unbiased screening by RNA-sequencing of flushed diaphyseal femoral bone and subsequent validation with qRT-PCR revealed that components of the Wnt signaling pathway were altered in *Girk3*$^{-/-}$ bone. For example, the mRNA transcripts for secreted Frizzled-related proteins (sFRP) family members sFRP4 and sFRP5 were reduced on day 4 of osteogenic differentiation in *Girk3*$^{-/-}$ BMSCs while sFRP3 expression was increased. sFRP4 and

5 are antagonists of Wnt signaling,[41,42] while sFRP3 is pro-osteogenic.[43] *Wnt6* was also upregulated in *Girk3*$^{-/-}$ mice. In contrast to other members of the Wnt family, *Wnt6* has been largely underexplored in bone development and disease. Perturbations mapped to the *WNT6* locus in the human genome have been associated with Acropectoro-vertebral dysplasia (F-syndrome), a rare skeletal disorder that includes symptoms such as carpal synostosis, syndactyly, and spina bifida occulta.[44] Inhibition of *Wnt6* in murine BMSCs enhances preadipocyte differentiation and inhibits osteogenesis in vitro.[45] As a variety of Wnt pathway regulators were affected by *Girk3* deletion, we chose to use a broad approach to inhibit Wnt signaling. Neither Dkk1 nor XAV939 reversed the increased proliferation in *Girk3*$^{-/-}$ BMSCs, but both inhibitors repressed *Girk3*$^{-/-}$ dependent enhanced mineralization in vitro. These data demonstrate that the mechanisms governing pro-proliferative activity in *Girk3*$^{-/-}$ BMSCs are distinct from those regulating elevated osteogenesis. In addition, enhanced osteogenesis was not completely reversed by Wnt canonical pathway inhibition in *Girk3*$^{-/-}$ cultures, indicating that *Girk3* also works through other mechanisms to enhance osteoblast activity and induce bone formation. Additional studies are necessary to define how *Girk3* deletion affects specific components of the Wnt signaling pathway and to understand the mechanisms underlying enhanced proliferation in *Girk3*$^{-/-}$ osteoblast progenitors.

Conditional deletion of *Girk3* in transgenic mice expressing Cre recombinase from the 2.3 kb-Col1a1 promoter was sufficient to recapitulate the high bone mass phenotype seen in *Girk3*$^{-/-}$ mice. The baseline bone parameters for WT mice and *Girk3*$^{fl/fl}$ mice are different, possibly due to differences in mouse substrain within our colony. Despite baseline differences, both global and 2.3 kb-Col1a1 conditional *Girk3* deletion increased trabecular bone mass relative to their respective controls. While the 2.3 kb-Col1a1 promoter is highly active in osteoblasts and osteocytes, it may also be active in neurons.[19,28,29,46] Thus, while the 2.3 kb-Col1a1 conditional knockout mouse is generally considered specific to osteoblasts,[28] the possibility that its expression in the small subset of 2.3 kb-Col1a1- and *Girk3*-co-expressing neuronal cells induces high bone mass cannot be excluded. An alternative possibility is that *Girk3* has a bone-cell-autonomous role, as bone cells are directly affected by ion channel activity. For example, Piezo1/2 and transient receptor potential family channels are indispensable for bone cell metabolism and transducing mechanical signals.[47] Additional studies are needed to determine the effect of neuronal *Girk3* on bone phenotypes.

Cortical bone mass and bone strength were elevated in 24-week-old *Girk3*-CKO$_{2.3Col1a1}$ mice in addition to trabecular bone mass, while *Girk3*$^{-/-}$ animals only showed elevated trabecular bone mass. Additionally, histomorphometry detected definitive increases in osteoblast number along trabecular surfaces in *Girk3*-CKO$_{2.3Col1a1}$ animals, whereas no differences were detected in *Girk3*$^{-/-}$ animals. These data indicate that osteoblast-directed *Girk3* deletion may induce bone accrual to an even greater extent than whole-body *Girk3* deletion. Bone formation by osteoblasts is balanced by osteoclastic bone resorption. Germline deletion of *Girk3* may therefore have conflicting or compensatory effects on multiple cell types in the bone microenvironment, while 2.3 kb-Col1a1 deletion allows for directed targeting. In addition to being highly expressed in the central nervous system, *Girk3* may also play a role in immune cell response and inflammation.[48] Indeed, RNA-Seq demonstrated the interferon activated gene *Ifi202b* mRNA expression was dramatically increased in *Girk3*$^{-/-}$ flushed diaphyseal bone. Interferon-activated *Ifi202b* and its human orthologue *IFI16* belong to the p200 family of transcriptional modulators, which play roles in cell proliferation, differentiation, and inflammation.[49] In the musculoskeletal system, *Ifi202b* promotes osteogenesis in BMSC cultures through induction of *Runx2* signaling.[50] As osteoclast number was modestly, but non-significantly, reduced in *Girk3*$^{-/-}$ compared to WT mice, it is possible that *Girk3* deletion may regulate hematopoiesis and osteoclastic bone resorption. More sensitive and specific assays examining the functions of *Girk3* in osteoclast and osteoclast progenitor cells are needed to further identify their contributions to the bone mass phenotypes of *Girk3* deficient mice.

At 4 weeks of age, trabecular bone mass was comparable between male *Girk3*-CKO$_{2.3Col1a1}$ mice and control littermates, similar to the pattern seen in *Girk3*$^{-/-}$ mice.[23] Cortical bone was thinner in 4-week-old *Girk3*-CKO$_{2.3Col1a1}$ mice compared to *Girk3*$^{fl/fl}$ littermates due to an unknown cellular mechanism, which will be the focus of future studies. By 24 weeks of age, however, analysis of the cortical bone revealed that the periosteal perimeter was greater in *Girk3*-CKO$_{2.3Col1a1}$ mice, while there was no difference in the endosteal perimeter, indicating appositional bone accrual. Further thresholding the cortical bone into low, medium, and high densities revealed that the newer, low-density and medium-density bone areas were greater in *Girk3*-CKO$_{2.3Col1a1}$ mice. The increased area of low- and medium-density cortical bone in *Girk3*-CKO$_{2.3Col1a1}$ animals accounts for the lower overall cortical TMD in these mice. However, the newer, lower density cortical bone in *Girk3*-CKO$_{2.3Col1a1}$ mice is not of compromised quality, as the low- and medium-density bone is positively correlated with increased bone strength. Taken together, conditional loss of *Girk3* in osteoblasts induces late-onset bone accrual, demonstrating a similar mechanism of action as germline *Girk3* deletion.

Both germline and 2.3 kb-Col1a1-directed *Girk3* deletion induce late-onset bone mass accrual. These data support previous work showing late-onset bone mass gains in mice with inhibited $G_{i/o}$ signaling.[7,8] As such, pharmacological inhibition of *Girk3* and/or $G_{i/o}$ inhibition are potential therapeutic strategies to increase bone mass in adults. While small-molecule GIRK channel activators and repressors have been developed, none target *Girk3* specifically.[16] Future work should be directed at identifying the effects of *Girk3* deletion on $G_{i/o}$ signaling to identify the therapeutic potential of targeting these signaling cascades together or independently to induce bone formation in adults.

In summary, our results define *Girk3* as a novel regulator of bone accrual in adulthood. Deletion of *Girk3* increases trabecular bone mass in male mice at 24 weeks of age. Bone marrow stromal cells from *Girk3*$^{-/-}$ animals are more proliferative and osteogenic in vitro. Conditional deletion of *Girk3* in osteoblasts is sufficient to induce high bone mass in adult male mice. Our findings introduce *Girk3* as a new player in the field of adult bone homeostasis, with potential connections to the central nervous and other systems that are open avenues of exploration.

Acknowledgments

We are grateful to the Augusta University Electron Microscopy & Histology Core who completed all histomorphometry, with support from their P01 Functional Outcomes Core (P01-AG036675-B) and Caihong Dai and Joseph C. Shaver. The authors would also like to thank the Mayo Clinic X-ray Imaging Resources Core Facility for use of the microCT scanner and the Mayo Clinic Biomechanics Core for performing 3-point bend tests.

Author contributions

Samantha Weaver (Conceptualization, Data curation, Formal analysis, Funding acquisition, Investigation, Methodology, Project administration, Validation, Writing—original draft, Writing—review & editing), Haydee Torres (Data curation, Formal analysis, Writing—review & editing), Katherine Arnold (Data curation, Formal analysis, Methodology, Writing—review & editing), Elizabeth Zars (Data curation, Writing—review & editing), Eduardo Peralta-Herrera (Data curation, Writing—review & editing), Earnest Taylor (Conceptualization, Writing—review & editing), Kanglun Yu (Data curation, Writing—review & editing), Ezequiel Marron Fernandez de Velasco (Conceptualization, Writing—review & editing), Kevin Wickman (Conceptualization, Writing—review & editing), Meghan McGee-Lawrence (Data curation, Formal analysis, Resources, Writing—review & editing), Elizabeth Bradley (Conceptualization, Writing—review & editing), and Jennifer Westendorf (Conceptualization, Formal analysis, Funding acquisition, Project administration, Resources, Supervision, Validation, Writing—original draft, Writing—review & editing)

Supplementary material

Supplementary material is available at *JBMR Plus* online.

Funding

This work was supported by research and training grants from the National Institutes of Health to S.R.W. (K99AR080745), J.J.W./K.W. (R21AR82134), and H.M.T. (T32AR056950). Funding and support were also provided by P01-AG036675-B, the Mayo Clinic Robert and Arlene Kogod Center on Aging and the Mayo Clinic Graduate School of Biomedical Sciences.

Conflicts of interest

The authors declare no conflict of interest.

Data availability

The transcriptomic data underlying this article are available in the Gene Expression Omnibus at https://www.ncbi.nlm.nih.gov/geo/ and can be accessed with Accession Number GSE264200. These and other data underlying this article are also available in the article and in its online supplementary material.

References

1. Lu J, Shin Y, Yen MS, Sun SS. Peak bone mass and patterns of change in total bone mineral density and bone mineral contents from childhood into young adulthood. *J Clin Densitom*. 2016;19(2):180–191. https://doi.org/10.1016/j.jocd.2014.08.001
2. Baxter-Jones AD, Faulkner RA, Forwood MR, Mirwald RL, Bailey DA. Bone mineral accrual from 8 to 30 years of age: an estimation of peak bone mass. *J Bone Miner Res*. 2011;26(8):1729–1739. https://doi.org/10.1002/jbmr.412
3. Josephson AM, Bradaschia-Correa V, Lee S, et al. Age-related inflammation triggers skeletal stem/progenitor cell dysfunction. *Proc Natl Acad Sci USA*. 2019;116(14):6995–7004. https://doi.org/10.1073/pnas.1810692116
4. Khosla S, Oursler MJ, Monroe DG. Estrogen and the skeleton. *Trends Endocrinol Metab*. 2012;23(11):576–581. https://doi.org/10.1016/j.tem.2012.03.008
5. Khosla S. Update in male osteoporosis. *J Clin Endocrinol Metab*. 2010;95(1):3–10. https://doi.org/10.1210/jc.2009-1740
6. Gaur T, Hussain S, Mudhasani R, et al. Dicer inactivation in osteoprogenitor cells compromises fetal survival and bone formation, while excision in differentiated osteoblasts increases bone mass in the adult mouse. *Dev Biol*. 2010;340(1):10–21. https://doi.org/10.1016/j.ydbio.2010.01.008
7. Millard SM, Wang L, Wattanachanya L, et al. Role of osteoblast Gi signaling in age-related bone loss in female mice. *Endocrinology*. 2017;158(6):1715–1726. https://doi.org/10.1210/en.2016-1365
8. Millard SM, Louie AM, Wattanachanya L, Wronski TJ, Conklin BR, Nissenson RA. Blockade of receptor-activated G(i) signaling in osteoblasts in vivo leads to site-specific increases in cortical and cancellous bone formation. *J Bone Miner Res*. 2011;26(4):822–832. https://doi.org/10.1002/jbmr.273
9. Logothetis DE, Kurachi Y, Galper J, Neer EJ, Clapham DE. The beta gamma subunits of GTP-binding proteins activate the muscarinic K+ channel in heart. *Nature*. 1987;325(6102):321–326. https://doi.org/10.1038/325321a0
10. Wickman KD, Iñiguez-Lluhl JA, Davenport PA, et al. Recombinant G-protein beta gamma-subunits activate the muscarinic-gated atrial potassium channel. *Nature*. 1994;368(6468):255–257. https://doi.org/10.1038/368255a0
11. Luján R, Fernandez M, de Velasco E, Aguado C, Wickman K. New insights into the therapeutic potential of Girk channels. *Trends Neurosci*. 2014;37(1):20–29. https://doi.org/10.1016/j.tins.2013.10.006
12. Anderson A, Kulkarni K, Fernandez M, et al. Expression and relevance of the G protein-gated K(+) channel in the mouse ventricle. *Sci Rep*. 2018;8(1):1192. https://doi.org/10.1038/s41598-018-19719-x
13. Blednov YA, Stoffel M, Chang SR, Harris RA. Potassium channels as targets for ethanol: studies of G-protein-coupled inwardly rectifying potassium channel 2 (GIRK2) null mutant mice. *J Pharmacol Exp Ther*. 2001;298(2):521–530.
14. Lyu C, Lyu GW, Mulder J, Martinez A, Shi TS. G protein-gated inwardly rectifying potassium channel subunit 3 is upregulated in rat DRGs and spinal cord after peripheral nerve injury. *J Pain Res*. 2020;13:419–429. https://doi.org/10.2147/JPR.S233744
15. Signorini S, Liao YJ, Duncan SA, Jan LY, Stoffel M. Normal cerebellar development but susceptibility to seizures in mice lacking G protein-coupled, inwardly rectifying K+ channel GIRK2. *Proc Natl Acad Sci USA*. 1997;94(3):923–927. https://doi.org/10.1073/pnas.94.3.923
16. Zhao Y, Gameiro-Ros I, Glaaser IW, Slesinger PA. Advances in targeting GIRK channels in disease. *Trends Pharmacol Sci*. 2021;42(3):203–215. https://doi.org/10.1016/j.tips.2020.12.002
17. Perry CA, Pravetoni M, Teske JA, et al. Predisposition to late-onset obesity in GIRK4 knockout mice. *Proc Natl Acad Sci USA*. 2008;105(23):8148–8153. https://doi.org/10.1073/pnas.0803261105
18. Mulatero P, Monticone S, Rainey WE, Veglio F, Williams TA. Role of KCNJ5 in familial and sporadic primary aldosteronism. *Nat Rev Endocrinol*. 2013;9(2):104–112. https://doi.org/10.1038/nrendo.2012.230
19. Oh Y, Yoo ES, Ju SH, et al. GIRK2 potassium channels expressed by the AgRP neurons decrease adiposity and body weight in mice. *PLoS Biol*. 2023;21(8):e3002252. https://doi.org/10.1371/journal.pbio.3002252
20. Hance MW, Dhar MS, Plummer HK 3rd. G-protein inwardly rectifying potassium channel 1 (GIRK1) knockdown decreases beta-adrenergic, MAP kinase and Akt signaling in the MDA-MB-453 breast cancer cell line. *Breast Cancer (Auckl)*. 2008;1:25–34. https://doi.org/10.4137/BCBCR.S629

21. Iwanir S, Reuveny E. Adrenaline-induced hyperpolarization of mouse pancreatic islet cells is mediated by G protein-gated inwardly rectifying potassium (GIRK) channels. *Pflugers Arch*. 2008;456(6):1097–1108. https://doi.org/10.1007/s00424-008-0479-4
22. Shankar H, Kahner BN, Prabhakar J, Lakhani P, Kim S, Kunapuli SP. G-protein–gated inwardly rectifying potassium channels regulate ADP-induced cPLA2 activity in platelets through Src family kinases. *Blood*. 2006;108(9):3027–3034. https://doi.org/10.1182/blood-2006-03-010330
23. Taylor EL, Weaver SR, Lorang IM, et al. GIRK3 deletion facilitates kappa opioid signaling in chondrocytes, delays vascularization and promotes bone lengthening in mice. *Bone*. 2022;159:116391. https://doi.org/10.1016/j.bone.2022.116391
24. Ng LF, Kaur P, Bunnag N, et al. WNT signaling in disease. *Cells*. 2019;8(8):826. https://doi.org/10.3390/cells8080826
25. Monroe DG, McGee-Lawrence ME, Oursler MJ, Westendorf JJ. Update on Wnt signaling in bone cell biology and bone disease. *Gene*. 2012;492(1):1–18. https://doi.org/10.1016/j.gene.2011.10.044
26. Miller SA, St Onge EL, Whalen KL. Romosozumab: a novel agent in the treatment for postmenopausal osteoporosis. *J Pharm Technol*. 2021;37(1):45–52. https://doi.org/10.1177/8755122520967632
27. Torrecilla M, Marker CL, Cintora SC, Stoffel M, Williams JT, Wickman K. G-protein-gated potassium channels containing Kir3.2 and Kir3.3 subunits mediate the acute inhibitory effects of opioids on locus ceruleus neurons. *J Neurosci*. 2002;22(11):4328–4334. https://doi.org/10.1523/JNEUROSCI.22-11-04328.2002
28. Liu F, Woitge HW, Braut A, et al. Expression and activity of osteoblast-targeted Cre recombinase transgenes in murine skeletal tissues. *Int J Dev Biol*. 2004;48(7):645–653. https://doi.org/10.1387/ijdb.041816fl
29. Couasnay G, Madel M-B, Lim J, Lee B, Elefteriou F. Sites of Cre-recombinase activity in mouse lines targeting skeletal cells. *J Bone Miner Res*. 2021;36(9):1661–1679. https://doi.org/10.1002/jbmr.4415
30. Mattson AM, Begun DL, Molstad DHH, et al. Deficiency in the phosphatase PHLPP1 suppresses osteoclast-mediated bone resorption and enhances bone formation in mice. *J Biol Chem*. 2019;294(31):11772–11784. https://doi.org/10.1074/jbc.RA119.007660
31. Walker EC, McGregor NE, Chan ASM, Sims NA. Measuring bone volume at multiple densities by micro-computed tomography. *Bio Protoc*. 2021;11(1):e3873. https://doi.org/10.21769/BioProtoc.3873
32. Walker EC, Truong K, McGregor NE, et al. Cortical bone maturation in mice requires SOCS3 suppression of gp130/STAT3 signalling in osteocytes. *elife*. 2020;9:e56666. https://doi.org/10.7554/eLife.56666
33. Pierce JL, Sharma AK, Roberts RL, et al. The glucocorticoid receptor in osterix-expressing cells regulates bone mass, bone marrow adipose tissue, and systemic metabolism in female mice during aging. *J Bone Miner Res*. 2022;37(2):285–302. https://doi.org/10.1002/jbmr.4468
34. McGee-Lawrence ME, Carpio LR, Bradley EW, et al. Runx2 is required for early stages of endochondral bone formation but delays final stages of bone repair in Axin2-deficient mice. *Bone*. 2014;66:277–286. https://doi.org/10.1016/j.bone.2014.06.022
35. Maridas DE, Rendina-Ruedy E, Le PT, Rosen CJ. Isolation, culture, and differentiation of bone marrow stromal cells and osteoclast progenitors from mice. *J Vis Exp*. 2018;6(131):56750. https://doi.org/10.3791/56750-v
36. McGee-Lawrence ME, Bradley EW, Dudakovic A, et al. Histone deacetylase 3 is required for maintenance of bone mass during aging. *Bone*. 2013;52(1):296–307. https://doi.org/10.1016/j.bone.2012.10.015
37. Livak KJ, Schmittgen TD. Analysis of relative gene expression data using real-time quantitative PCR and the 2(-Delta Delta C(T)) method. *Methods*. 2001;25(4):402–408. https://doi.org/10.1006/meth.2001.1262
38. Bagi CM, Hanson N, Andresen C, et al. The use of micro-CT to evaluate cortical bone geometry and strength in nude rats: correlation with mechanical testing, pQCT and DXA. *Bone*. 2006;38(1):136–144. https://doi.org/10.1016/j.bone.2005.07.028
39. Papageorgiou M, Föger-Samwald U, Wahl K, Kerschan-Schindl K, Pietschmann P. Age- and strain-related differences in bone microstructure and body composition during development in inbred male mouse strains. *Calcif Tissue Int*. 2020;106(4):431–443. https://doi.org/10.1007/s00223-019-00652-8
40. Wang L, Hsiao EC, Lieu S, et al. Loss of Gi G-protein-coupled receptor signaling in osteoblasts accelerates bone fracture healing. *J Bone Miner Res*. 2015;30(10):1896–1904. https://doi.org/10.1002/jbmr.2540
41. Haraguchi R, Kitazawa R, Mori K, et al. sFRP4-dependent Wnt signal modulation is critical for bone remodeling during postnatal development and age-related bone loss. *Sci Rep*. 2016;6(1):25198. https://doi.org/10.1038/srep25198
42. He HP, Gu S. The PPAR-γ/SFRP5/Wnt/β-catenin signal axis regulates the dexamethasone-induced osteoporosis. *Cytokine*. 2021;143:155488. https://doi.org/10.1016/j.cyto.2021.155488
43. Katagiri W, Osugi M, Kawai T, Hibi H. Secreted frizzled-related protein promotes bone regeneration by human bone marrow-derived mesenchymal stem cells. *Int J Mol Sci*. 2015;16(10):23250–23258. https://doi.org/10.3390/ijms161023250
44. Huybrechts Y, Mortier G, Boudin E, van Hul W. WNT signaling and bone: lessons from skeletal dysplasias and disorders. *Front Endocrinol*. 2020;11:165. https://doi.org/10.3389/fendo.2020.00165
45. Cawthorn WP, Bree AJ, Yao Y, et al. Wnt6, Wnt10a and Wnt10b inhibit adipogenesis and stimulate osteoblastogenesis through a β-catenin-dependent mechanism. *Bone*. 2012;50(2):477–489. https://doi.org/10.1016/j.bone.2011.08.010
46. Scheller EL, Leinninger GM, Hankenson KD, Myers MG Jr, Krebsbach PH. Ectopic expression of Col2.3 and Col3.6 promoters in the brain and association with leptin signaling. *Cells Tissues Organs*. 2011;194(2-4):268–273. https://doi.org/10.1159/000324745
47. Zhang K, Liu X, Wang L, et al. The mechanosensory and mechanotransductive processes mediated by ion channels and the impact on bone metabolism: a systematic review. *Arch Biochem Biophys*. 2021;711:109020. https://doi.org/10.1016/j.abb.2021.109020
48. Zhang H, Cao S, Xu Y, et al. Landscape of immune infiltration in entorhinal cortex of patients with Alzheimer's disease. *Front Pharmacol Orig Res*. 2022;13:941656. https://doi.org/10.3389/fphar.2022.941656
49. Choubey D, Duan X, Dickerson E, et al. Interferon-inducible p200-family proteins as novel sensors of cytoplasmic DNA: role in inflammation and autoimmunity. *J Interf Cytokine Res*. 2010;30(6):371–380. https://doi.org/10.1089/jir.2009.0096
50. Zhang L, Wang C, Zhang X, Li H. The interferon-inducible protein p202 promotes osteogenesis in mouse bone marrow stromal cells. *Biosci Rep*. 2018;38(3):BSR20171618. https://doi.org/10.1042/BSR20171618